Title: Targeting the Cx26/NANOG/Focal Adhesion Kinase Complex via Cell Penetrating Peptides in Triple Negative Breast Cancers

Authors: Emily L. Esakov[1], Erin E. Mulkearns Hubert [1,2], Rashmi Bharti [1], Sarah Johnson[1], Smarajit Bandyopadhyay [3], Erinn Downs-Kelly[4], Justin D. Lathia[1,2,5]*, Ofer Reizes[1,2,5,]*

Affiliations:

[1]Department of Cardiovascular and Metabolic Sciences, Cancer Impact Area, Lerner Research Institute, Cleveland Clinic Foundation, 9500 Euclid Avenue, Cleveland, Ohio 44195.

[2]Department of Molecular Medicine, Cleveland Clinic Lerner College of Medicine of Case Western Reserve University, 9500 Euclid Avenue, Cleveland, Ohio 44195

[3]Molecular Biotechnology Core, Lerner Research Institute, Cleveland Clinic Foundation, 9500 Euclid Avenue, Cleveland, Ohio 44195.

[4]Department of Pathology, Cleveland Clinic Foundation, 9500 Euclid Avenue, Cleveland, Ohio 44195

[5]Case Comprehensive Cancer Center, 10900 Euclid Ave. Cleveland, OH 44106

*Co-senior and Co-Corresponding authors.

To whom correspondence should be addressed: Ofer Reizes, reizeso@ccf.org; Justin Lathia, lathiaj@ccf.org

One Sentence Summary: A peptide-based targeting strategy for triple-negative breast cancer was developed by targeting connexin 26-associated signaling partners.

Abstract

Purpose: Triple-negative breast cancer (TNBC) represents the most lethal and treatment-resistant breast cancer subtype and has limited treatment options. We previously identified a protein complex unique to TNBC cancer stem cells composed of the gap junction protein connexin 26 (Cx26), the pluripotency transcription factor NANOG, and focal adhesion kinase (FAK). We sought to determine whether a peptide mimetic of Cx26 designed to target the complex could attenuate tumor growth in pre-clinical models.

Experimental Design: Histological assessment was employed to verify expression of complex members. We designed peptides based on Cx26 juxtamembrane domains and performed binding experiments with NANOG and FAK using surface plasmon resonance. Peptides with high affinity were engineered with a cell-penetrating sequence and assessed in functional assays including cell proliferation, self-renewal, and in vivo tumor growth, and downstream signaling changes were measured.

Results: Binding studies revealed that the Cx26 cytoplasmic C-terminal tail and intracellular loop bound to NANOG and FAK with submicromolar to micromolar affinity and that a 5-amino acid sequence in the C-terminal tail of Cx26 (RYCSG) was sufficient for binding. An antennapedia cell penetrating peptide sequence was engineered to the Cx26 C-terminal tail and confirmed intracellular localization. The cell-penetrating Cx26 C-terminal tail peptide (aCx26-pep) disrupted self-renewal as assessed by the tumorsphere formation assay and inhibited NANOG target gene expression in TNBC cells but not in luminal mammary epithelial cells. In a pre-clinical setting, aCx26-pep reduced tumor growth and proliferation and induced cell death.

Conclusions: We provide proof-of-concept that a Cx26 peptide-based strategy can inhibit TNBC growth.

Translational Relevance (150 words)

Triple-negative breast cancer (TNBC) is the most treatment-refractory breast cancer subtype and has limited targeted therapy options. TNBC contains a cancer stem cell (CSC) population that underlies growth and therapeutic resistance. We leveraged an aberrant intracellular protein complex in TNBC CSCs containing the gap junction subunit connexin 26 (Cx26), focal adhesion kinase (FAK), and NANOG to develop a peptide-based therapeutic strategy. We show that TNBC can be selectively targeted using this approach. Our findings provide a new strategy for treatment of this patient population by disrupting intracellular Cx26 signaling, which is linked to the CSC and epithelial-to-mesenchymal programs. Our results support the development of therapeutics targeting the Cx26/NANOG/FAK complex via peptide- and small molecule-based approaches, and future efforts will also focus on the development of a combinatorial treatment strategy with FDA-approved chemotherapeutics.

Introduction

Triple-negative breast cancer (TNBC), the most aggressive breast cancer subtype, is associated with high rates of recurrence and metastasis[1-5]. To date, unlike other breast cancer subtypes, no specific targeted approaches exist for TNBC, and toxic chemotherapeutic agents are the primary treatment regimen, highlighting the need to develop new targeted therapies. TNBC contains a high degree of cellular heterogeneity and plasticity that has emerged as a hallmark of the malignant state and accounts for the observed persistent tumor growth, therapeutic resistance, and metastasis[6-9]. TNBC also contains self-renewing, therapeutically resistant cancer stem cells (CSCs) that are responsible for tumor progression and metastasis[10-13]. Given the limited treatment options for TNBC, CSC neutralizing strategies are an immediate priority for therapeutic development.

Attempts to elucidate the complexity of CSC maintenance have focused on intrinsic driver mutations and altered developmental signaling pathways[14]. The elevated cellular density within tumors stimulates cellular programs that are activated by cell-cell contact and close proximity. The gap junction family of proteins is composed of connexin subunits and canonically functions in gap junction plaques at the interface of adjacent cells to facilitate direct cell-cell communication. Connexins can also function non-canonically as single membrane channels (hemichannels, which contain a single assembled connexon hexamer of connexins) or as signaling hubs adjacent to any organelle and/or the plasma membrane[15]. In cancer, the classical role of connexins as tumor suppressors has been widely described in many tumor models[16-20]. However, the paradigm that connexins have a global tumor-suppressive role has been challenged by recent evidence that connexins can be pro-tumorigenic by facilitating tumor progression and metastasis[21-27]. The connexin subunits involved in maintaining homeostasis during the physiological development and function of the mammary gland are Cx26 and Cx43[18, 28]. In breast cancer, connexins have been described to be both pro- and anti-tumorigenic by regulating transformation, proliferation, cell survival, and metastasis[27]. Most studies to date suggest a tumor-suppressive role for Cx26 early in breast cancer progression based on evidence that Cx26 is frequently absent or down-regulated in human breast cancer cell lines and human primary tumors[15, 29-31]. However, these studies are inconsistent with clinical observations that demonstrate a strong correlation between increased Cx26 expression in breast cancer tissue samples post-treatment (chemotherapy/surgery) and decreased overall survival[32]. Moreover, Cx26 expression has been shown to be associated with increased lymphatic vessel invasion, increased tumor size, and poor prognosis in human breast cancers[32, 33].

We previously demonstrated that Cx26 is elevated in TNBC compared to normal mammary tissue and enriched in CSCs compared to their non-CSC progeny in TNBC cell lines and patient-derived xenograft models[34]. In functional studies, we demonstrated that Cx26 is necessary and sufficient for CSC maintenance and regulates NANOG protein stability. In TNBC, Cx26 localizes to an intracellular membrane-bound vesicle in complex with the pluripotency transcription factor NANOG and focal adhesion kinase (FAK). In contrast to its role in the normal mammary epithelium, Cx26 functions in a gap junction-independent manner in TNBC by forming an intracellular complex that underlies the maintenance of CSC function and stabilizes NANOG. We leveraged these initial findings to develop a peptide-based strategy to disrupt this novel signaling network. We developed peptides to the intracellular and extracellular regions of Cx26 and identified the binding domains necessary for interaction with NANOG and FAK. Using a cell-penetrating peptide strategy, we show that introduction of the Cx26 C-terminus into TNBC cells inhibits self-renewal, reduces NANOG target gene expression, and attenuates in vivo tumor growth. Together, this study provides proof-of-concept that targeting CSCs via connexin peptide mimetics represent a viable therapeutic strategy for TNBC.

Results

The Cx26/NANOG/FAK complex is present in patient TNBC samples

Previous data from our group identified a protein complex unique to TNBC CSCs composed of the gap junction protein connexin 26 (Cx26), the pluripotency transcription factor NANOG, and focal adhesion kinase (FAK) [34]. To assess whether the Cx26/NANOG/FAK complex is also present in patient tumors, we stained sections of human triple-negative invasive ductal carcinoma for Cx26, NANOG, and FAK. Hematoxylin & eosin staining showed the invasive nature of the tumors (**Fig. 1A**). In cultured TNBC cells, we found that Cx26 localizes to an intracellular compartment rather than the canonical plasma membrane localization of connexins[34]. Consistently, we observed intracellular localization of staining for Cx26, NANOG, and FAK in adjacent tumor sections of TNBC patient tumor (**Fig. 1B-D**). In contrast, tumor samples from patients with hormone receptor positive and HER2 negative tumors showed cell surface localization of Cx26 distinct from NANOG and FAK (**Fig. 1E-H**). This indicates that Cx26, NANOG, and FAK have similar subcellular localizations, suggesting that the complex may be present in TNBC patient tumors as well as in cells, as we previously described[34].

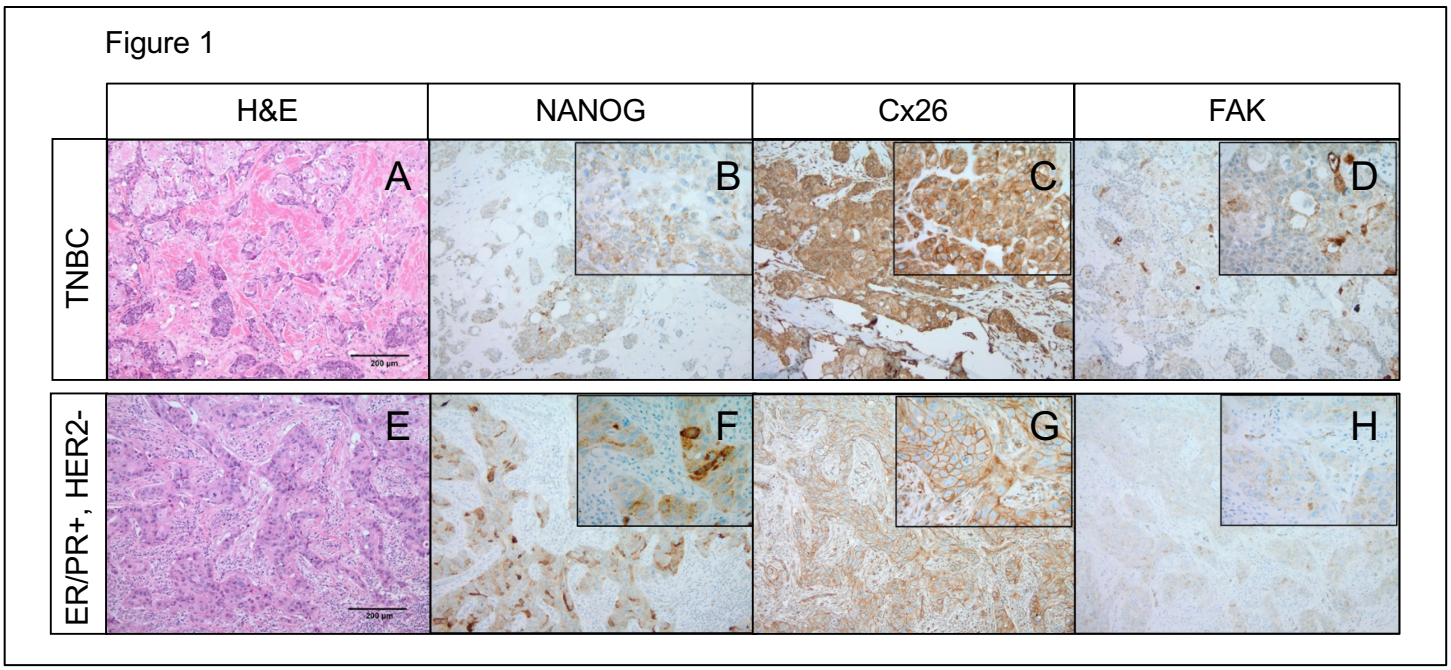

Figure 1. Cx26, NANOG, and FAK localize to intracellular compartment in TNBC tumors. A-D: TNBC assessed by sequential whole slides as stained with A) Hematoxylin and eosin showing an invasive ductal carcinoma with focal squamous differentiation, Nottingham grade 3, B) NANOG stain showing weak cytoplasmic expression within tumor cells (inset showing granular cytoplasmic staining in a large subset of the tumor cells), C) Cx26 stain showing intense cytoplasmic staining within a majority of the tumor cells (inset showing higher

magnification) and D) FAK stain showing weak granular cytoplasmic staining within a subset of tumor cells (inset showing weak granular cytoplasmic staining and darker accentuation of staining in area of squamous differentiation). E-H: Estrogen/progesterone receptor (ER/PR)+/HER2- tumor assessed by sequential whole slides stained with E) Hematoxylin and eosin showing an invasive ductal carcinoma, Nottingham grade 3, F) NANOG immunohistochemical stain showing variable cytoplasmic expression within tumor cells (inset showing both weak and more intense foci of cytoplasmic staining), G) Cx26 immunohistochemical stain showing circumferential membranous expression on tumor cells (inset showing moderate to strong diffuse membrane staining) and H) FAK immunohistochemical stain showing very weak granular cytoplasmic staining within tumor cells (inset showing weak but diffuse granular cytoplasmic staining). Photomicrograph total magnification for each pane is 100x; inset total magnification is 400x.

Sequential whole tissue sections of 33 different invasive ductal carcinomas were examined by IHC. Briefly, all twelve TNBC tumors had variable intensity (weak to strong) predominately cytoplasmic but also focally membranous staining for Cx26 in greater than 60% of tumor cells. Of these, 4 had variable-intensity cytoplasmic staining with FAK, and 5 had variable nuclear or cytoplasmic staining for NANOG. Five hormone receptor (estrogen/progesterone receptors; HR)-/HER2+ carcinomas were included and all showed variable intensity (weak to strong) cytoplasmic staining in 40-90% of tumor cells for Cx26 as well as cytoplasmic expression of both NANOG and FAK. Four HR+/HER2+ carcinomas were studied, with half showing weak to moderate cytoplasmic and membranous staining of Cx26 in 90% of the tumor cells and the other two cases showing weak membranous staining only in > 60% of tumor cells. Of the cases with only membranous Cx26 expression, 2 cases had no expression of FAK and 1 had weak cytoplasmic expression of FAK. The 2 cases with cytoplasmic and membranous expression of Cx26 both had variable (weak to moderate) cytoplasmic expression of FAK and NANOG. Twelve HR+/HER2- carcinomas were evaluated, and 7 showed weak to intense membranous only staining with Cx26 within >90% of tumor cells. The remaining cases showed moderate-intensity membranous and cytoplasmic staining for Cx26. Of the cases with Cx26 membranous staining only, 6 showed variable (weak to moderate intensity) cytoplasmic expression of FAK in 5-90% of tumor cells while 5 showed variable (weak to moderate intensity) expression of NANOG in 5-90% of tumor cells. Of the 5 cases showing moderate intensity membranous and cytoplasmic staining with Cx26, 4 showed variable

(weak to moderate intensity) cytoplasmic expression of FAK in 50-90% of tumor cells, while NANOG was similarly expressed, with weak to moderate cytoplasmic expression in 5% - 90% of tumor cells.

FAK and NANOG interact with the cytosolic tail of Cx26

Based on the essential role for the Cx26/NANOG/FAK complex in TNBC CSC maintenance[34], targeting the complex represents a therapeutic opportunity. To develop therapies targeting the complex, we used surface plasmon resonance (SPR) to interrogate the specific domains through which the proteins interact. We generated peptide fragments representing the intracellular and extracellular domains of Cx26 and determined their ability to bind to either FAK or NANOG by SPR. The strongest binding occurred between NANOG and the Cx26 cytosolic tail and between FAK and both the cytosolic tail and the cytosolic loop, with dissociation constants in the nanomolar and micromolar ranges, respectively (**Fig. 2A**). Importantly, no binding was observed between the FAK and NANOG proteins alone (**Fig. 2A**). These observations combined with predictive modeling suggesting that complex binding requires Cx26, as we detected binding between Cx26 and NANOG, Cx26 and FAK, and all members of the complex but not between FAK and NANOG alone (**Supplemental Fig. 1**). This informed a binding schematic for the Cx26/NANOG/FAK complex (**Fig. 2B**) where NANOG binds to the C-terminus while FAK interacts with both the C-terminus and the intracellular loop of Cx26. To determine the specific Cx26 cytosolic tail amino acid residues important for binding, various truncations of the C-terminal tail were synthesized and subjected to SPR analysis for binding to both NANOG and FAK. The minimal required region mapped to Cx26 amino acids 216-220 (**Supplemental Table 1 and Supplemental Fig. 2**). To gain more insight into the kinetics of binding, we co-incubated the Cx26 cytosolic tail with NANOG prior to applying the components to a FAK-bound chip. We also performed this analysis with Cx26 cytosolic tail pre-incubated with FAK prior to applying to a NANOG-bound chip. Interestingly, the Cx26 cytosolic tail had decreased binding affinity for both FAK and NANOG when pre-incubated with the other complex member compared to the Cx26 cytosolic tail alone or pre-incubation with bovine serum albumin control (not shown). Taken together, these data indicate that NANOG and FAK binding to the Cx26 tail may be competitive.

Figure 2

A

Analyte	Ligand	Dissociation constant (KD)
Cytosolic loop	FAK	1.13^{-5} M
Cytosolic tail	FAK	4.48^{-8} M
Cytosolic tail	NANOG	8.75^{-8} M
FAK	NANOG	> 1.00 M

B

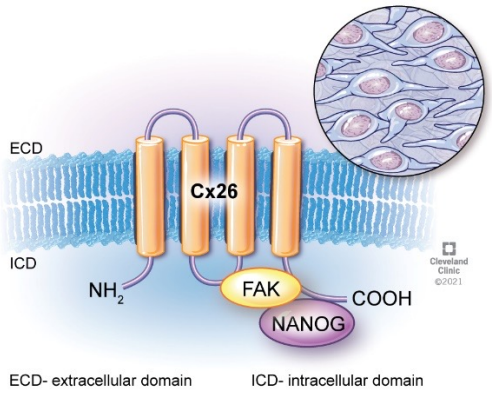

C

Analyte	Ligand	Dissociation constant (KD)
Antennapedia (Antp) RQIKIWFQNRRMKWKK	FAK	>1M
	NANOG	>1M
Antp-cytosolic tail (aCx26-pep) (RQIKIWFQNRRMKWKK-RYCSGKSKKPV)	FAK	8.39^{-8} M
	NANOG	8.75^{-8} M
Antp-scrambled cytosolic tail (aScr-pep) (RQIKIWFQNRRMKWKK-KVCLKDSGKTT)	FAK	>1M
	NANOG	>1M
Extracellular loop 2 (YVMYDGFSMQRLVKCNAWPCPNTVDCFVSRPTEKTVFT)	FAK	>1M
	NANOG	>1M
Antp-extracellular loop 2 (RQIKIWFQNRRMKWKK-YVMYDGFSMQRLVKCNAWPCPNTVDCFVSRPTEKTVFT)	FAK	>1M
	NANOG	>1M

D

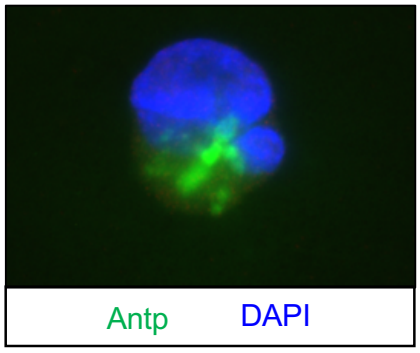

E

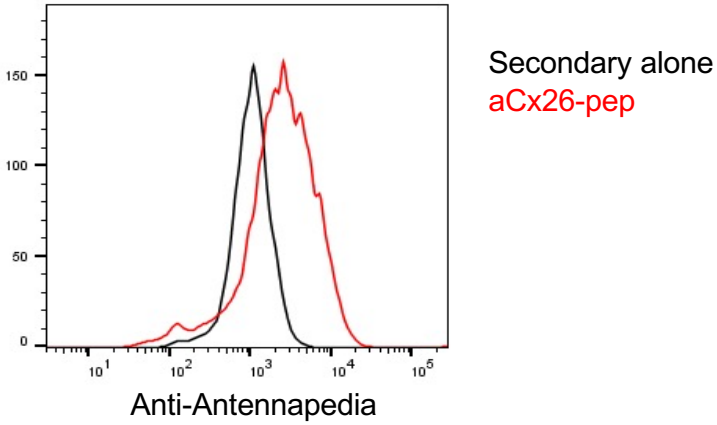

Figure 2. Cx26 cytosolic tail peptide binds both FAK and NANOG and can penetrate the cell membrane upon addition of an antennapedia (Antp) leader sequence. A. Table denoting dissociation constants for interactions between Cx26 and NANOG and FAK. B. Cartoon depiction of complex based on SPR analysis. C. Summary table of FAK and NANOG dissociation constants with Antp alone, tagged cytosolic tail, or tagged cleaved tail peptides by SPR analysis. D. Immunofluorescence staining and E. intracellular flow cytometry

staining for Antp following 10 μM aCx26-pep treatment, demonstrating the ability of the peptide to cross the plasma membrane.

Based on the observation that the Cx26 cytosolic tail is essential for interaction with NANOG and FAK, we sought to understand the effect of disrupting the complex using a Cx26 cytosolic tail-derived cell-penetrating peptide. We tagged a peptide containing the Cx26 cytosolic tail sequence with an antennapedia (Antp) (RQIKIWFQNRRMKWKK) leader sequence (termed hereafter aCx26-pep). Antp is a well-studied leader sequence used to allow peptides and small molecules to penetrate the plasma membrane[35]. aCT1, a Cx43 C-terminal tail mimetic peptide, impairs the malignant progression of luminal breast cancer cells and enhances the activity of the standard-of-care chemotherapies lapatinib and tamoxifen[36, 37]. We first confirmed that the Antp leader sequence did not significantly alter the ability of aCx26-pep to bind to either FAK or NANOG by SPR (**Fig. 2C and Supplemental Fig. 3**). To determine the optimal treatment conditions, cells were assessed for the presence of aCx26-pep by intracellular immunofluorescence (IF) staining **(Fig. 2D)** and flow cytometry (**Fig. 2E**) using an anti-Antp antibody, and optimal treatment conditions were determined to be 10 μM peptide for a minimum of 3 hours.

Self-renewal but not proliferation of TNBC cells is attenuated by aCx26-pep treatment

To assess the functional effects of treatment, we evaluated cell proliferation and self-renewal in TNBC cells treated with aCx26-pep in vitro. MDA-MB-231 TNBC cells were treated with increasing doses of vehicle, Antp alone, and aCx26-pep, and cell proliferation was measured after 72 hours of treatment. Interestingly, cell proliferation was not significantly affected by treatment with aCx26-pep (**Fig. 3A, B**). To assess changes in self-renewal, tumorsphere formation was interrogated in three TNBC cell lines (MDA-MB-231, MDA-MB-468 and HCC70) and one luminal breast cancer cell line (MCF7) treated with vehicle, Antp, aScr-pep, and aCx26-pep. Tumorsphere initiation frequency was assessed using an extreme limiting dilution assay (ELDA) and subsequent ELDA analysis software [38]. TNBC cells treated with aCx26-pep had significantly decreased tumorsphere frequency compared to those treated with aScr-pep, whereas the luminal breast cancer cell line showed no significant difference between aScr-pep and aCx26-pep (**Fig. 3 C-F. and Supplemental Table 2**). Together, these data show that disrupting the Cx26/NANOG/FAK complex using aCx26-pep decreases the self-renewal capacity of TNBC cells.

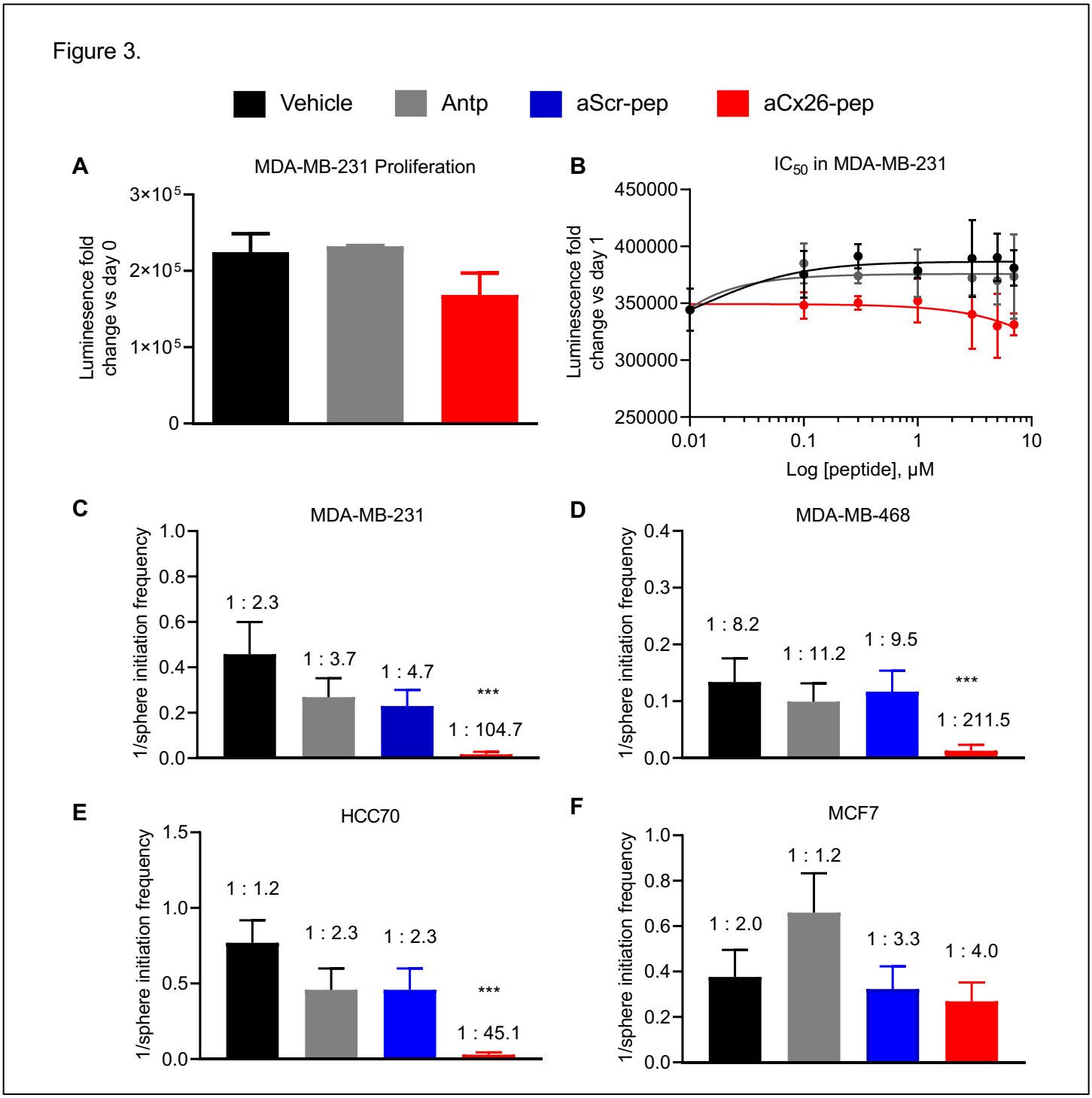

Figure 3. TNBC self-renewal but not cell proliferation is attenuated following aCx26-pep treatment. Cell proliferation measured by CellTiter Glo is not significantly affected by aCx26-pep treatment compared to controls over time (A) or by concentration of peptide (B). Tumorsphere initiation frequency is decreased in MDA-MB-231 (C), MDA-MB-468 (D), and HCC70 (E) TNBC cells treated with aCx26-pep compared to vehicle, Antp alone, or aScr-pep controls but is not affected in MCF7 luminal breast cancer cells (F). *** $p<0.001$.

aCx26-pep treatment attenuates NANOG target gene expression

To further understand the downstream signaling changes following treatment of TNBC cells with aCx26-pep, we performed a targeted qPCR assessment of NANOG-regulated genes. Following 10 days of treatment with vehicle, aScr-pep, or aCx26-pep, expression of NANOG target genes including *FABP5*, *POSTN*, *NRP2*, *PIN1*, and *TAGLN* was significantly decreased in MDA-MB-231 TNBC cells treated with aCx26-pep compared to those treated with vehicle or aScr-pep (**Fig. 4A**). Expression of epithelial cell markers such as cytokeratin 18 and 19 (*KRT18* and *KRT19*) was significantly increased in the aCx26-pep treatment group (**Fig. 4B**). In contrast, treatment of MCF7 luminal breast cancer cells did not significantly change NANOG target gene or cytokeratin gene expression (**Fig. 4C-D**). Together, these results indicate decreased transcriptional activity of NANOG and an increase in epithelial cell signature after treatment with aCx26-pep.

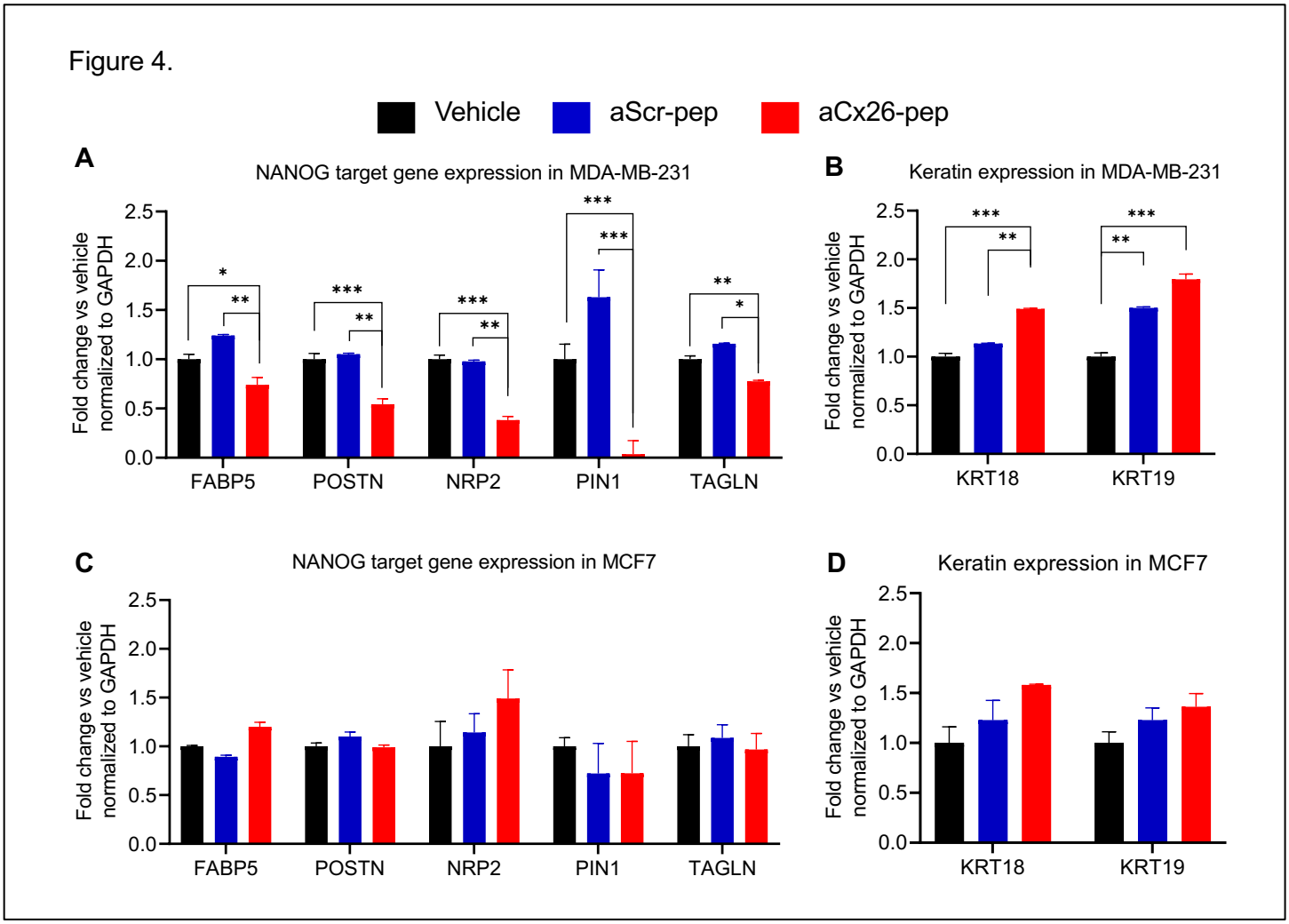

Figure 4. NANOG target genes enriched in CSCs are decreased when MDA-MB-231 cells are treated with aCx26-pep. A. Following a 7 day treatment with 10 μM aCx26-pep, MDA-MB-231 cells had decreased expression of genes regulated by NANOG by qPCR compared to cells treated with either cytosolic tail peptide alone, aScr-pep or vehicle alone. There were no significant differences in gene expression between the vehicle, cytosolic tail, or aScr-pep groups. * $p<0.05$, ** $p<0.01$, *** $p<0.001$.

In vivo TNBC tumor progression is attenuated by aCx26-pep

To determine the effect of aCx26-pep on tumor formation *in vivo*, NSG mice were subcutaneously injected into the flank with TNBC MDA-MB-231 luciferase-expressing cells and randomized into treatment groups once tumors became palpable. Mice were intra-tumorally injected every other day for 20 days with either vehicle, aScr-pep, or aCx26-pep and monitored by weekly bioluminescence imaging (**Fig. 5A**). Mice treated with aCx26-pep exhibited significantly reduced luciferase signal (tumor burden) over time when compared to those treated with aScr-pep or vehicle controls (**Fig. 5B, C**).

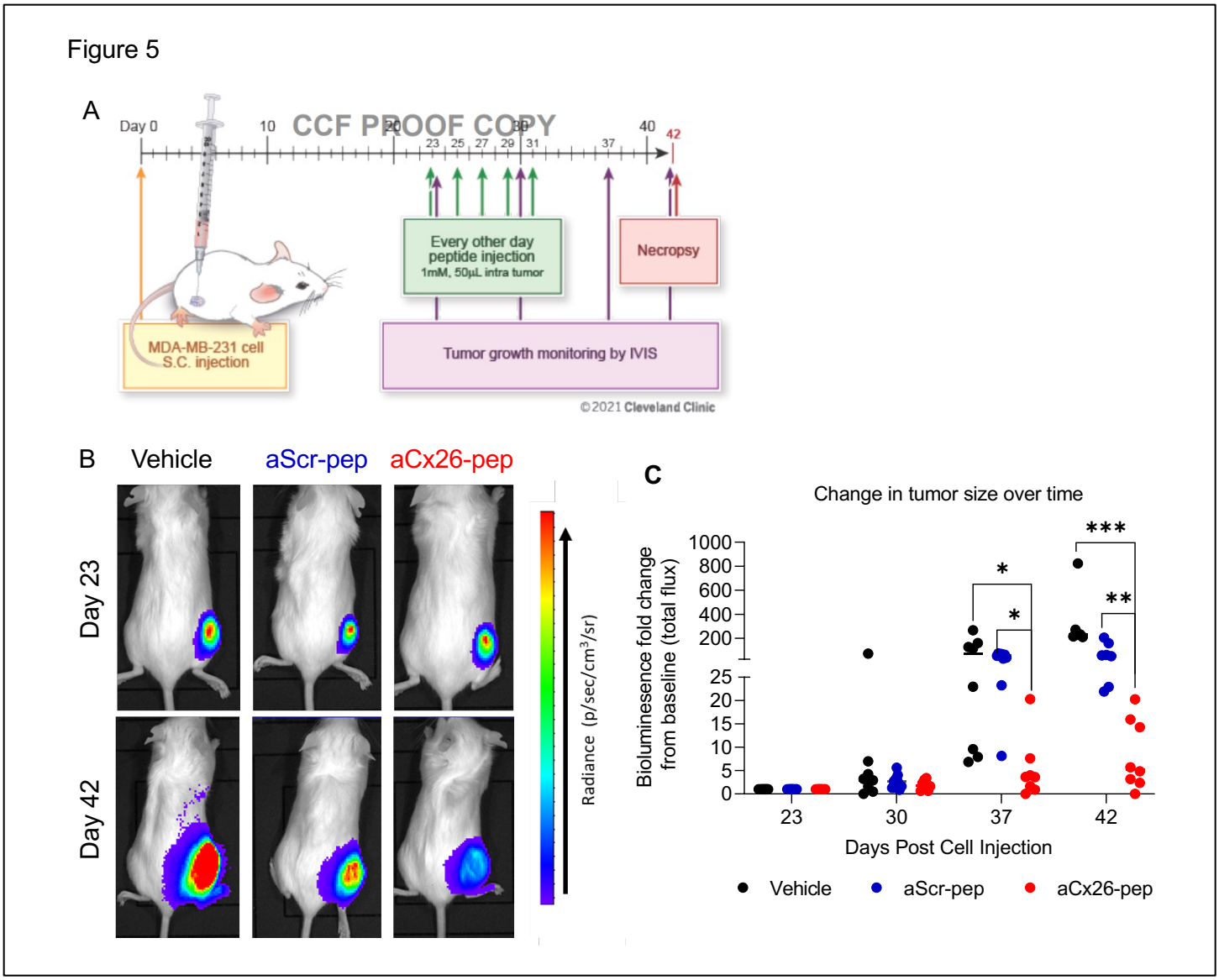

Figure 5. Tumor growth is attenuated upon aCx26-pep treatment *in vivo.* A. Following palpability of tumors in the subcutaneous right flank generated by MDA-MB-231 cell injection, mice were intratumorally treated with 1 mM vehicle, aScr-pep or aCx26-pep every other day for 20 days and monitored by weekly IVIS imaging. B. Representative IVIS images of treated mice at Day 0 and Day 42. C. Tumors treated with aCx26-pep exhibited attenuated proliferation over time compared to control groups. n=8 mice per group; $p<0.05$, ** $p<0.01$, *** $p<0.001$.

We then performed histological assessment of the resulting tumors. Upon H&E staining of isolated tumors, we observed that the percent tumor viability was significantly decreased in aCx26-pep-treated mice compared to vehicle- or aScr-pep-treated mice (**Fig. 6A**). Immunofluorescence staining of the endpoint tumors showed that Ki67 (**Fig. 6B**), a marker for proliferation, and vimentin (**Fig. 6C**), a marker for epithelial-mesenchymal transition (EMT), were decreased, while cleaved caspase 3 was increased (**Fig. 6D**), in the aCx26-pep-treated groups,

suggesting that peptide treatment led to a more epithelial cell phenotype with increased cell death and diminished proliferation.

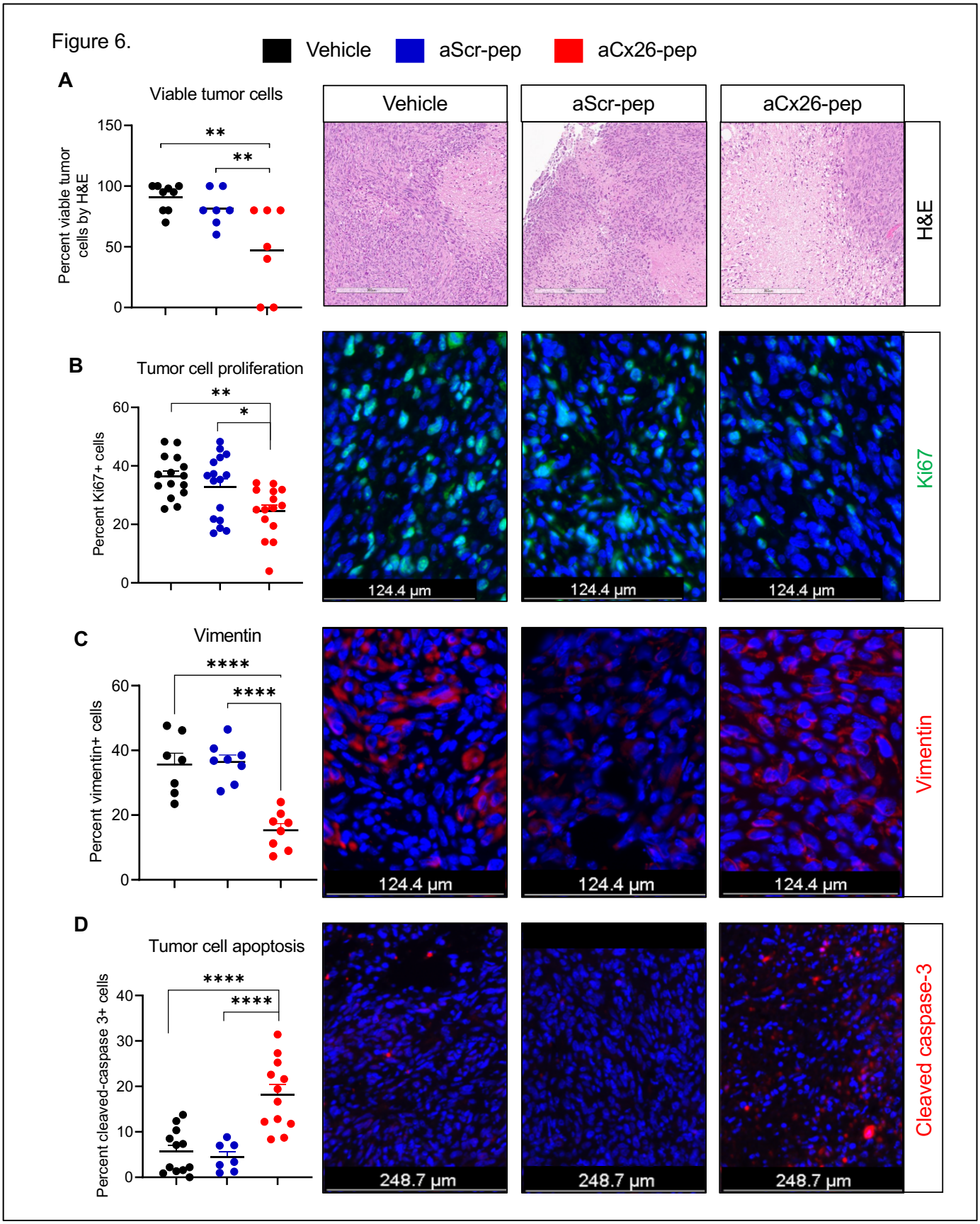

Figure 6. aCx26-pep-treated tumors show decreased tumor proliferation and cell viability and increased cell death. At endpoint, aCx26-pep-treated tumors exhibited diminished viability by H&E scoring (A), decreased Ki67 staining (B), decreased vimentin expression (C), and increased cleaved caspase 3 expression (D) compared to tumors treated with either aScr-pep or vehicle. H&E: 7-8 mice per group, IF staining: 3-4 mice per group, 3 images per mouse. Scales bars are as denoted in each image. One way ANOVA *$p<0.05$, **$p<0.01$, ***$p<0.005$, ****$p<0.0001$.

Discussion

Overall, our findings provide proof-of-concept data that a peptide strategy can be employed to reduce CSC self-renewal and tumor growth. We leveraged previous observations of the Cx26/NANOG/FAK complex in TNBC to develop a pre-clinical peptide-based targeting strategy to attenuate CSC function. Our studies focused solely on CSCs and tumor growth, key cancer phenotypes that likely involve FAK and NANOG. However, given the number of downstream signaling networks associated with FAK and NANOG, there are likely to be other cellular programs that may also be driven by their association with Cx26, including adhesion, migration, and invasion. An additional unanswered question is the possibility of differential functions of free and Cx26-complex-bound NANOG and FAK.

Immunohistochemical analysis complemented our breast cancer cell line data, with the majority of TNBC specimens having cytoplasmic expression of Cx26 with a subset exhibiting co-localization of FAK and NANOG. In contrast, the majority of HR+/HER2- carcinomas showed membranous expression of Cx26 and cytoplasmic localization of FAK and NANOG. The distinct cellular localization of Cx26 expression in TNBC and HR+/HER2- tumors further supports the hypothesis that therapeutic targeting of Cx26 would benefit this aggressive tumor subtype. Although the immunohistochemical TNBC data are not as compelling as those seen in the TNBC cell lines, FFPE immunohistochemistry may suffer from antibody affinity, fixation issues and antigen retrieval. Clinical outcomes data related to a larger cohort defined with Cx26, FAK and NANOG will be helpful in further elucidating this complex and its role.

Our findings identify a strategy to disrupt CSC phenotypes by blocking intracellular Cx26 interactions via a cell-penetrating peptide approach. A challenge in targeting connexin family members remains specificity, as there is a high degree of structural homology among connexin family members, apart from the cytoplasmic tail that provides a binding surface for adaptor proteins to initiate signaling programs. In previous work, the cytoplasmic tail of Cx43 was found to associate with zona occludens-1 (ZO-1) to exclude assembled connexins from the gap junction plaque; disruption of the interaction with ZO-1 resulted in an increase in gap junction intracellular communication[37]. A peptide mimetic of this region of the Cx43 tail tagged with antennapedia has been successfully leveraged to enhance diabetic would healing and is in advanced stages of clinical testing[39]. These findings provided the first example that peptides can be used to modulate intracellular connexin function for a

clinically relevant application. Our findings provide the first evidence of the utility of this application for CSC targeting and potential downstream signaling modulation. While these peptide-based approaches show promise, there remain barriers to implementation, including delivery and stability. Future studies will focus on addressing these key limitations to facilitate clinical translation.

Targeting CSCs remains of interest in many cancers, including TNBC, but many late-stage trials are focused on canonical developmental programs (including Sonic hedgehog, Wnt, and Notch). Next-generation strategies are more likely to be successful if they can leverage CSC-specific signaling networks. CSC targeting represents a new cancer therapeutic development pipeline that is complementary to oncogene addiction targeting and tumor suppressor re-expression. Connexins and their main functions of cell-cell communication, hemichannel communication, and initiation of signaling have been largely understudied in the context of cancer and may represent a new therapeutic target. These findings highlight a selective strategy using a peptide approach to target TNBC, leading to new therapeutic options for the unmet need in this patient population.

Materials and Methods

Study Approvals

All mouse procedures were performed under adherence to protocols approved by the Institute Animal Care and Use Committee at the Lerner Research Institute, Cleveland Clinic (#2018-2101). All human specimens were obtained under adherence to protocols approved by the Cleveland Clinic Foundation Institutional Review Board (IRB approval #17-418).

TNBC Cx26, FAK, and NANOG histology and analysis

Annotated cases of invasive ductal carcinoma were retrieved from the surgical pathology files of Cleveland Clinic and included triple negative breast carcinoma (TNBC), hormone receptor positive (HR+ being estrogen receptor positive) and HER2 negative (HR+/HER2-), hormone receptor negative (HR- being estrogen receptor negative) and HER2 positive (HR-/HER2+) or hormone receptor positive and HER2 positive (HR+/HER2+). In total, 12 TNBC, 12 HR+/HER2-, 5 HR-/HER2+, 4 HR+/HER2+ tumors were evaluated. Hematoxylin and eosin stained slides were reviewed for invasive tumor adequacy and immunohistochemistry (IHC) was performed on 4-μm thick formalin-fixed paraffin-embedded (FFPE) whole tissue serial sections following antigen retrieval (Target Retrieval Solution, pH 6.1; Dako, Carpinteria, CA). Immunostains performed included Connexin 26 (Cx26) mouse monoclonal antibody (clone CX-12H10, Thermo Fisher Scientific, Waltham, MA) at 1:200 dilution, NANOG rabbit monoclonal antibody (clone EPR2027, Abcam, Cambridge, MA) at 1:250 dilution, and FAK rabbit polyclonal antibody (clone Q05397, Cell Signaling Technology, Danvers, MA) at 1:500 dilution. All staining was performed on an automated platform (Ventana Benchmark, Ultraview XT, Ventana Medical Systems, Inc, Tucson, AZ) and visualized with ultraView universal DAB detection kit (Ventana Medical Systems, Inc, Tucson, AZ). The cellular compartment staining (membranous, cytoplasmic or nuclear) was evaluated and the intensity in each case for the three antibodies was characterized as weak, moderate, or strong, and the extent of immunoreactivity scored according to the percentage of tumor cells with staining: 0 (0%), 1+ (<5%), 2+ (5–25%), 3+ (26–50%), 4+ (51–75%), and 5+ (76–100%).

Cell Culture

MDA-MB-231, MDA-MB-468, HCC70, and MCF7 breast cancer cells (American Type Culture Collection; Manassas, VA) were cultured in log-growth phase in Dulbecco's modified Eagle's medium (DMEM) supplemented with 1 mM sodium pyruvate (Cellgro, Kansas City, MO) and 10% heat-inactivated fetal calf serum (FCS) at 37°C in a humidified atmosphere (5% CO_2). All cell lines were authenticated through the Cleveland Clinic Lerner Research Institute Cell Culture Core and routinely tested for mycoplasma contamination.

Peptide Synthesis and Validation

All peptides, unless otherwise noted, were synthesized by the LRI Molecular Biotechnology Core through standard solid-phase chemistry, using Rink Amide resin and side chain-protected Fmoc-amino acids, on a Liberty Blue Automated Microwave Peptide Synthesizer (CEM Corporation, Matthews, NC). Each peptide was purified to > 95% by acetonitrile gradient elution (20 - 50%) on a Vydac preparative C18 column, using reverse-phase HPLC (Waters Corporation). The quality of the peptide was analyzed by HPLC (Agilent 1100) on a reverse-phase analytical C-18 column. The correct mass corresponding to the amino acid composition of each peptide was then confirmed by mass spectrometry (MALDI-TOF/TOF mass spectrometer; Model No. 4800; AB SCIEX, Framingham, MA). The peptides were lyophilized and stored at -80°C until reconstituted in 1% DMSO/PBS.

Surface Plasmon Resonance (SPR) Analysis

The equilibrium dissociation constants (KD) between synthesized Cx26 cytosolic tail peptides and either NANOG or FAK proteins were determined using the Biacore X100 (GE Healthcare, Sweden) at 25°C. The 1% DMSO/1x PBS buffer was filtered through a 0.22-μm membrane filter and degassed immediately before the experiment as running buffer with a flow rate of 30 μL/min for the instrument system. The purified active NANOG was diluted in 10 mM sodium acetate solution pH 4.5, resulting in a protein concentration of 50 μg/mL, and purified active FAK was diluted in 10 mM sodium acetate solution pH 3.0, resulting in a protein concentration of 20 μg/mL. The diluted protein was immobilized on the surface of a CM5 sensor chip via the primary amine group, employing a standard Amine Coupling Kit (1-Ethyl-3-(3-dimethylaminopropyl)-carbodiimide hydrochloride (EDC), N-hydroxysuccinimide (NHS) and 1.0 M ethanolamine-HCl (pH 8.5)), and the target immobilization level was 5000

response units (RUs). The flow cell 1 without any modification was used as a reference to correct for system error. The RU values were collected, and all the binding affinity data were calculated by kinetic models (1:1 Langmuir interaction) within the Biacore X100 Evaluation Software. To determine the binding affinity between each peptide and NANOG or FAK, a series of peptide protein dilutions was analyzed by multi-cycle kinetics/affinity. A concentration gradient of each peptide as the analyte was freshly prepared in running buffer at at least five concentrations (100 nM – 100 μM). Each peptide at various gradient concentrations (including a repeat concentration) and one zero concentration (running buffer) flowed over the immobilized NANOG or FAK, with 120 s for binding, followed by disassociation for 120 s, and the obtained RUs were recorded. After the injection of each concentration of each peptide, the sensor chip surface was regenerated with 10 mM glycine pH 2.5 for 30 s to completely remove the residual peptide. The KD was calculated to evaluate the ability of peptides to interact with NANOG or FAK proteins.

Immunofluorescence and Flow Cytometry Analysis of Antp-peptides

Following aCx26-pep treatment, MDA-MB-231 and MCF7 cells were lifted and washed in 1x PBS followed by staining with UV Live/Dead dye (1:1000, Thermo Scientific) for 15 minutes at room temperature. Cells were then fixed and permeabilized using the Annexin V Staining Kit (BD Biosciences) per the manufacturer's instructions and incubated with FITC-conjugated anti-antennapedia (anti-Antp-FITC) antibody (1:100, LSBio) for 30 minutes. Samples were washed and analyzed using a BD Fortessa flow cytometer. MDA-MB-231 cells were plated onto glass coverslips in 6-well plates and treated with aCx26-pep (10 μM) for 3 hours. Subsequently, coverslips were washed with 1x PBS and stained with anti-antennapedia antibody (anti-Antp 4C3, 1:500, University of Iowa Developmental Studies Hybridoma Bank) for 1 hour at room temperature. Coverslips were washed twice with 1x PBS and stained with Texas Red-conjugated anti-mouse secondary (1:1000, Invitrogen) for 1 hour at room temperature in the dark, before being mounted in DAPI mount (VWR) onto glass slides and imaged with a confocal microscope at 20x magnification (Leica). Appropriate secondary alone controls were completed to confirm the absence of background staining. Data analysis was performed using the FlowJo software v10 (Tree Star, Inc., Ashland, OR).

CellTiter Glo Proliferation Studies

MDA-MB-231 cells were plated in a 96-well (opaque-walled) plates at 1,000 cells/well and treated for 72 hours with Antp peptide alone, aCx26-pep or vehicle (1% DMSO in PBS) at the concentrations shown in the figures. At day 0 and post 72 hours of treatment, cells were lysed with CellTiter-Glo® Luminescent Cell Viability Assay reagent (Promega), shaken in the dark for 10 minutes, and luminescence was recorded. Fold change was calculated by normalizing the 72 hour luminescence value to day 0 for each group.

Self-renewal (Tumorsphere) Assays

Duplicate rows of cells were cultured in serial dilutions per well (1-20 cells per well) in one 96-well plate (Sarstedt, Germany) per condition with 200 µl serum-free DMEM supplemented with 20 ng/ml basic fibroblast growth factor (Invitrogen, Grand Island, NY), 10 ng/ml epidermal growth factor (BioSource, Grand Island, NY), 2% B27 (Invitrogen, Grand Island, NY), 10 µg/ml insulin, and 1 µg/ml hydrochloride (Sigma, Saint Louis, MO). The frequency of sphere formation was calculated in such a way that a well with a tumorsphere was counted as a positive well and a well with no tumorspheres was counted as a negative well. Tumorspheres were counted under a phase contrast microscope after 2 weeks. The stem cell frequencies were calculated using an extreme limiting dilution algorithm (http://bioinf.wehi.edu.au/software/elda/)[38].

Real-time Quantitative PCR

Quantitative polymerase chain reaction (qPCR) was performed using a StepOnePlus™ Real-Time PCR System (Applied Bioystems) with SYBR-Green MasterMix (SA Biosciences). RNA was extracted using the RNeasy kit (Qiagen, Limburg, Netherlands), and cDNA was synthesized using the Superscript III kit (Invitrogen, Grand Island, NY). For qPCR analysis, the threshold cycle (CT) values for each gene were normalized to expression levels of GAPDH. Dissociation curves were evaluated for primer fidelity. The primers used are detailed in Supplemental Table 1.

Animal Studies

NOD.Cg-Prkdc^{scid} Il2rg^{tm1Wjl}/SzJ (NSG) female mice were purchased from Jackson Laboratories or the Biological Resource Unit at the Lerner Research Institute, Cleveland Clinic. All mice were maintained in microisolator units and provided free access to food and water. MDA-MB-231 cells were transduced with a luciferase lentiviral vector

(pHIV-Luciferase, Addgene #21375). Following puromycin drug selection, $1x10^6$ cells were injected into the right subcutaneous flank of 6-week-old female mice. Once tumors became palpable, mice were randomized into groups and received either 1 mM aCx26-pep, aScr-pep, or vehicle (1% DMSO) via intra-tumoral injection every other day for 20 days. Tumor progression was assessed weekly via bioluminescent IVIS imaging (see below). Following treatment regiment, mice were euthanized by CO_2 asphyxiation with subsequent cervical dislocation and necropsied for further analysis.

Bioluminescent IVIS Imaging

Bioluminescence images were taken with an IVIS Lumina (PerkinElmer) using D-luciferin as previously described[40]. Mice received an intraperitoneal (IP) injection of D-luciferin (Goldbio LUCK-1G, 150 mg/kg in 150 µL) under inhaled isoflurane anesthesia. Images were analyzed (Living Image Software), and total flux were reported in photons/second/cm^2/steradian for each mouse.

Immunohistochemistry

Upon necropsy, subcutaneous tumors were excised, sectioned and placed in 4% paraformaldehyde (PFA) for 3 days at room temperature, before being transferred into 70% ethanol and sent to the Histology Core at the LRI for processing, sectioning, and staining. Slides were imaged using the Aperio slide scanner and analyzed.

Statistical Analysis

Values reported in the results represent mean ± standard error of the mean (SEM). One-way analysis of variance was used to calculate statistical significance, and *p* values and replicate numbers are detailed in the text and figure legends.

References

1. Abdulkarim BS, Cuartero J, Hanson J, Deschenes J, Lesniak D and Sabri S. Increased risk of locoregional recurrence for women with T1-2N0 triple-negative breast cancer treated with modified radical mastectomy without adjuvant radiation therapy compared with breast-conserving therapy. *J Clin Oncol*. 2011;29:2852-8.
2. Al-Hajj M, Wicha MS, Benito-Hernandez A, Morrison SJ and Clarke MF. Prospective identification of tumorigenic breast cancer cells. *Proc Natl Acad Sci U S A*. 2003;100:3983-8.
3. Aslakson CJ and Miller FR. Selective events in the metastatic process defined by analysis of the sequential dissemination of subpopulations of a mouse mammary tumor. *Cancer research*. 1992;52:1399-405.
4. Greenberg PA, Hortobagyi GN, Smith TL, Ziegler LD, Frye DK and Buzdar AU. Long-term follow-up of patients with complete remission following combination chemotherapy for metastatic breast cancer. *J Clin Oncol*. 1996;14:2197-205.
5. Rakha EA, El-Sayed ME, Green AR, Lee AH, Robertson JF and Ellis IO. Prognostic markers in triple-negative breast cancer. *Cancer*. 2007;109:25-32.
6. Lawrence RT, Perez EM, Hernandez D, Miller CP, Haas KM, Irie HY, Lee SI, Blau CA and Villen J. The proteomic landscape of triple-negative breast cancer. *Cell Rep*. 2015;11:630-44.
7. Perou CM. Molecular stratification of triple-negative breast cancers. *Oncologist*. 2011;16 Suppl 1:61-70.
8. Lehmann BD, Bauer JA, Chen X, Sanders ME, Chakravarthy AB, Shyr Y and Pietenpol JA. Identification of human triple-negative breast cancer subtypes and preclinical models for selection of targeted therapies. *J Clin Invest*. 2011;121:2750-67.
9. Hudis CA and Gianni L. Triple-negative breast cancer: an unmet medical need. *Oncologist*. 2011;16 Suppl 1:1-11.
10. Charafe-Jauffret E, Ginestier C, Iovino F, Wicinski J, Cervera N, Finetti P, Hur MH, Diebel ME, Monville F, Dutcher J, Brown M, Viens P, Xerri L, Bertucci F, Stassi G, Dontu G, Birnbaum D and Wicha MS. Breast cancer cell lines contain functional cancer stem cells with metastatic capacity and a distinct molecular signature. *Cancer research*. 2009;69:1302-13.
11. Giatromanolaki A, Sivridis E, Fiska A and Koukourakis MI. The CD44+/CD24- phenotype relates to 'triple-negative' state and unfavorable prognosis in breast cancer patients. *Med Oncol*. 2011;28:745-52.
12. Idowu MO, Kmieciak M, Dumur C, Burton RS, Grimes MM, Powers CN and Manjili MH. CD44(+)/CD24(-/low) cancer stem/progenitor cells are more abundant in triple-negative invasive breast carcinoma phenotype and are associated with poor outcome. *Hum Pathol*. 2012;43:364-73.
13. Sheridan C, Kishimoto H, Fuchs RK, Mehrotra S, Bhat-Nakshatri P, Turner CH, Goulet R, Jr., Badve S and Nakshatri H. CD44+/CD24- breast cancer cells exhibit enhanced invasive properties: an early step necessary for metastasis. *Breast Cancer Res*. 2006;8:R59.
14. Martin-Castillo B, Lopez-Bonet E, Cuyas E, Vinas G, Pernas S, Dorca J and Menendez JA. Cancer stem cell-driven efficacy of trastuzumab (Herceptin): towards a reclassification of clinically HER2-positive breast carcinomas. *Oncotarget*. 2015;6:32317-38.
15. Stewart MK, Bechberger JF, Welch I, Naus CC and Laird DW. Cx26 knockout predisposes the mammary gland to primary mammary tumors in a DMBA-induced mouse model of breast cancer. *Oncotarget*. 2015;6:37185-99.
16. Lee SW, Tomasetto C and Sager R. Positive selection of candidate tumor-suppressor genes by subtractive hybridization. *Proc Natl Acad Sci U S A*. 1991;88:2825-9.
17. Cronier L, Crespin S, Strale PO, Defamie N and Mesnil M. Gap junctions and cancer: new functions for an old story. *Antioxid Redox Signal*. 2009;11:323-38.
18. Mesnil M. Connexins and cancer. *Biol Cell*. 2002;94:493-500.
19. Laird DW, Fistouris P, Batist G, Alpert L, Huynh HT, Carystinos GD and Alaoui-Jamali MA. Deficiency of connexin43 gap junctions is an independent marker for breast tumors. *Cancer research*. 1999;59:4104-10.
20. Janssen-Timmen U, Traub O, Dermietzel R, Rabes HM and Willecke K. Reduced number of gap junctions in rat hepatocarcinomas detected by monoclonal antibody. *Carcinogenesis*. 1986;7:1475-82.
21. Dobrowolski R, Sasse P, Schrickel JW, Watkins M, Kim JS, Rackauskas M, Troatz C, Ghanem A, Tiemann K, Degen J, Bukauskas FF, Civitelli R, Lewalter T, Fleischmann BK and Willecke K. The conditional connexin43G138R mouse mutant represents a new model of hereditary oculodentodigital dysplasia in humans. *Hum Mol Genet*. 2008;17:539-54.
22. el-Sabban ME and Pauli BU. Cytoplasmic dye transfer between metastatic tumor cells and vascular endothelium. *J Cell Biol*. 1991;115:1375-82.

23. Ito A, Katoh F, Kataoka TR, Okada M, Tsubota N, Asada H, Yoshikawa K, Maeda S, Kitamura Y, Yamasaki H and Nojima H. A role for heterologous gap junctions between melanoma and endothelial cells in metastasis. *J Clin Invest*. 2000;105:1189-97.
24. Ezumi K, Yamamoto H, Murata K, Higashiyama M, Damdinsuren B, Nakamura Y, Kyo N, Okami J, Ngan CY, Takemasa I, Ikeda M, Sekimoto M, Matsuura N, Nojima H and Monden M. Aberrant expression of connexin 26 is associated with lung metastasis of colorectal cancer. *Clin Cancer Res*. 2008;14:677-84.
25. Li Q, Omori Y, Nishikawa Y, Yoshioka T, Yamamoto Y and Enomoto K. Cytoplasmic accumulation of connexin32 protein enhances motility and metastatic ability of human hepatoma cells in vitro and in vivo. *Int J Cancer*. 2007;121:536-46.
26. Elzarrad MK, Haroon A, Willecke K, Dobrowolski R, Gillespie MN and Al-Mehdi AB. Connexin-43 upregulation in micrometastases and tumor vasculature and its role in tumor cell attachment to pulmonary endothelium. *BMC Med*. 2008;6:20.
27. A Gonçalves J-YP, E Brain, C Tarpin, H Cure, B Esterni, A Boyer-Chammard, F Bertucci, A Jalaguier, G Houvenaeghel, P Viens, E Charaffe-Jauffret, and J-M Extra. Abstract OT2-3-05: AVASTEM: a phase II randomized trial evaluating anti-cancer stem cell activity of pre-operative bevacizumab and chemotherapy in breast cancer. *Cancer research*. 2012;72.
28. McLachlan E, Shao Q and Laird DW. Connexins and gap junctions in mammary gland development and breast cancer progression. *J Membr Biol*. 2007;218:107-21.
29. Hirschi KK, Xu CE, Tsukamoto T and Sager R. Gap junction genes Cx26 and Cx43 individually suppress the cancer phenotype of human mammary carcinoma cells and restore differentiation potential. *Cell growth & differentiation : the molecular biology journal of the American Association for Cancer Research*. 1996;7:861-70.
30. Wilgenbus KK, Kirkpatrick CJ, Knuechel R, Willecke K and Traub O. Expression of Cx26, Cx32 and Cx43 gap junction proteins in normal and neoplastic human tissues. *Int J Cancer*. 1992;51:522-9.
31. Kanczuga-Koda L, Sulkowski S, Lenczewski A, Koda M, Wincewicz A, Baltaziak M and Sulkowska M. Increased expression of connexins 26 and 43 in lymph node metastases of breast cancer. *Journal of clinical pathology*. 2006;59:429-33.
32. Teleki I, Krenacs T, Szasz MA, Kulka J, Wichmann B, Leo C, Papassotiropoulos B, Riemenschnitter C, Moch H and Varga Z. The potential prognostic value of connexin 26 and 46 expression in neoadjuvant-treated breast cancer. *BMC Cancer*. 2013;13:50.
33. Naoi Y, Miyoshi Y, Taguchi T, Kim SJ, Arai T, Tamaki Y and Noguchi S. Connexin26 expression is associated with lymphatic vessel invasion and poor prognosis in human breast cancer. *Breast cancer research and treatment*. 2007;106:11-7.
34. Thiagarajan PS, Sinyuk M, Turaga SM, Mulkearns-Hubert EE, Hale JS, Rao V, Demelash A, Saygin C, China A, Alban TJ, Hitomi M, Torre-Healy LA, Alvarado AG, Jarrar A, Wiechert A, Adorno-Cruz V, Fox PL, Calhoun BC, Guan JL, Liu H, Reizes O and Lathia JD. Cx26 drives self-renewal in triple-negative breast cancer via interaction with NANOG and focal adhesion kinase. *Nat Commun*. 2018;9:578.
35. Sagan S, Burlina F, Alves ID, Bechara C, Dupont E and Joliot A. Homeoproteins and homeoprotein-derived peptides: going in and out. *Curr Pharm Des*. 2013;19:2851-62.
36. Grek CL, Rhett JM, Bruce JS, Abt MA, Ghatnekar GS and Yeh ES. Targeting connexin 43 with alpha-connexin carboxyl-terminal (ACT1) peptide enhances the activity of the targeted inhibitors, tamoxifen and lapatinib, in breast cancer: clinical implication for ACT1. *BMC Cancer*. 2015;15:296.
37. Hunter AW, Barker RJ, Zhu C and Gourdie RG. Zonula occludens-1 alters connexin43 gap junction size and organization by influencing channel accretion. *Mol Biol Cell*. 2005;16:5686-98.
38. Hu Y and Smyth GK. ELDA: extreme limiting dilution analysis for comparing depleted and enriched populations in stem cell and other assays. *J Immunol Methods*. 2009;347:70-8.
39. Zhang A, Hitomi M, Bar-Shain N, Dalimov Z, Ellis L, Velpula KK, Fraizer GC, Gourdie RG and Lathia JD. Connexin 43 expression is associated with increased malignancy in prostate cancer cell lines and functions to promote migration. *Oncotarget*. 2015;6:11640-51.
40. Chambers LM, Esakov E, Braley C, AlHilli M, Michener C and Reizes O. Use of Transabdominal Ultrasound for the detection of intra-peritoneal tumor engraftment and growth in mouse xenografts of epithelial ovarian cancer. *PLoS One*. 2020;15:e0228511.

Acknowledgements. The authors would like to thank members of the Lathia and Reizes laboratories for insightful comments during implementation of these studies. We appreciate the technical contributions of Chad Braley, members of the Lerner Genomics Shared Lab Resources, specifically Dr. Dean Horton, and the Imaging Core, namely Judith Drazba. The research was supported by the Department of Defense Grant W81XWH1910503, NIH R21 CA191263, and VeloSano Bike to Cure to Drs. Reizes and Lathia. Dr. Reizes is also supported by The Laura J. Fogarty Endowed Chair for Uterine Cancer Research.

Figure Legends

Figure 1. Cx26, NANOG, and FAK localize to intracellular compartment in TNBC tumors. A-D: TNBC assessed by sequential whole slides as stained with A) Hematoxylin and eosin showing an invasive ductal carcinoma with focal squamous differentiation, Nottingham grade 3, B) NANOG stain showing weak cytoplasmic expression within tumor cells (inset showing granular cytoplasmic staining in a large subset of the tumor cells), C) Cx26 stain showing intense cytoplasmic staining within a majority of the tumor cells (inset showing higher magnification) and D) FAK stain showing weak granular cytoplasmic staining within a subset of tumor cells (inset showing weak granular cytoplasmic staining and darker accentuation of staining in area of squamous differentiation). E-H: HR+/HER2- assessed by sequential whole slides stained with E) Hematoxylin and eosin showing an invasive ductal carcinoma, Nottingham grade 3, F) NANOG immunohistochemical stain showing variable cytoplasmic expression within tumor cells (inset showing both weak and more intense foci of cytoplasmic staining), G) Cx26 immunohistochemical stain showing circumferential membranous expression on tumor cells (inset showing moderate to strong diffuse membrane staining) and H) FAK immunohistochemical stain showing very weak granular cytoplasmic staining within tumor cells (inset showing weak but diffuse granular cytoplasmic staining). Photomicrographs total magnification for each pane is 100x, inset total magnification is 400x.

Figure 2. Cx26 cytosolic tail peptide binds both FAK and NANOG and can penetrate the cell membrane upon addition of an antennapedia (Antp) leader sequence. A. Table denoting dissociation constants for interactions between Cx26 and NANOG and FAK. B. Cartoon depiction of complex based on SPR analysis. C. Summary table of FAK and NANOG dissociation constants with Antp alone, tagged cytosolic tail, or tagged cleaved tail peptides by SPR analysis. D. Immunofluorescence staining and E. intracellular flow cytometry staining for Antp following 10 μM aCx26-pep treatment, demonstrating the ability of the peptide to cross the plasma membrane.

Figure 3. TNBC self-renewal but not cell proliferation is attenuated following aCx26-pep treatment. Cell proliferation measured by CellTiter Glo is not significantly affected by aCx26-pep treatment compared to controls over time (A) or by concentration of peptide (B). Tumorsphere initiation frequency is decreased in MDA-MB-231 (C), MDA-MB-468 (D), and HCC70 (E) TNBC cells treated with aCx26-pep compared to vehicle, Antp alone, or aScr-pep controls but is not affected in MCF7 luminal breast cancer cells (F). *** $p<0.001$.

Figure 4. NANOG target genes enriched in CSCs are decreased when MDA-MB-231 cells are treated with aCx26-pep. A. Following a 7 day treatment with 10 μM aCx26-pep, MDA-MB-231 cells had decreased expression of genes regulated by NANOG by qPCR compared to cells treated with either cytosolic tail peptide alone, aScr-pep or vehicle alone. There were no significant differences in gene expression between the vehicle, cytosolic tail, or aScr-pep groups. * $p<0.05$, ** $p<0.01$, *** $p<0.001$.

Figure 5. Tumor growth is attenuated upon aCx26-pep treatment *in vivo.* A. Following palpability of tumors in the subcutaneous right flank generated by MDA-MB-231 cell injection, mice were intratumorally treated with 1 mM vehicle, aScr-pep or aCx26-pep every other day for 20 days and monitored by weekly IVIS imaging. B. Representative IVIS images of treated mice at Day 0 and Day 42. C. Tumors treated with aCx26-pep exhibited attenuated proliferation over time compared to control groups. n=8 mice per group; $p<0.05$, ** $p<0.01$, *** $p<0.001$.

Figure 6. aCx26-pep-treated tumors show decreased tumor proliferation and cell viability and increased cell death. At endpoint, aCx26-pep-treated tumors exhibited diminished viability by H&E scoring (A), decreased Ki67 staining (B), decreased vimentin expression (C), and increased cleaved caspase 3 expression (D) compared to tumors treated with either aScr-pep or vehicle. H&E: 7-8 mice per group, IF staining: 3-4 mice per group, 3 images per mouse. Scales bars are as denoted in each image. One way ANOVA *$p<0.05$, **$p<0.01$, ***$p<0.005$, ****$p<0.0001$.

Supplemental Figures.

Supplemental Fig. S1

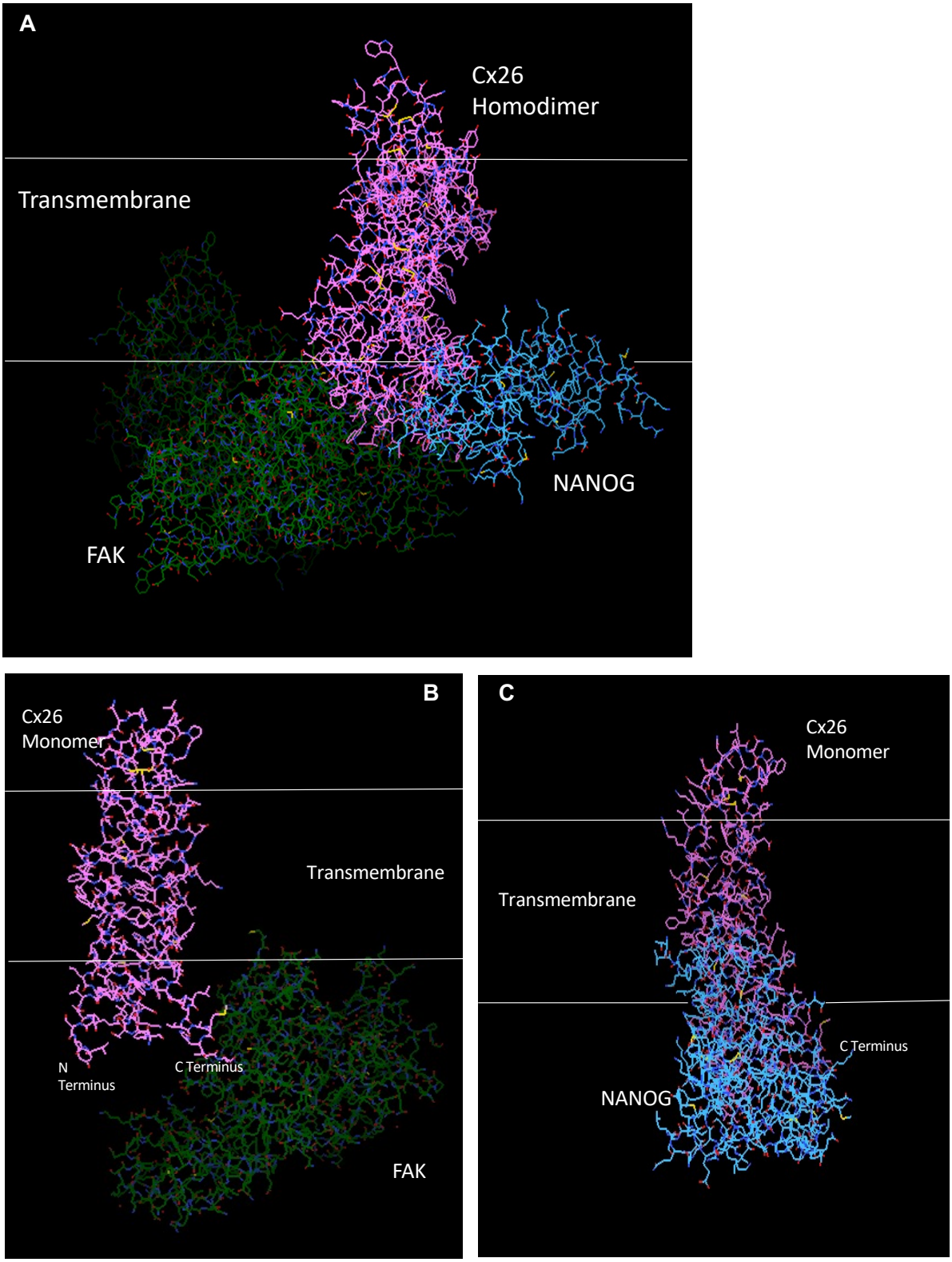

Supplemental Figure 1. Predicted model of Cx26 in complex with NANOG and FAK.

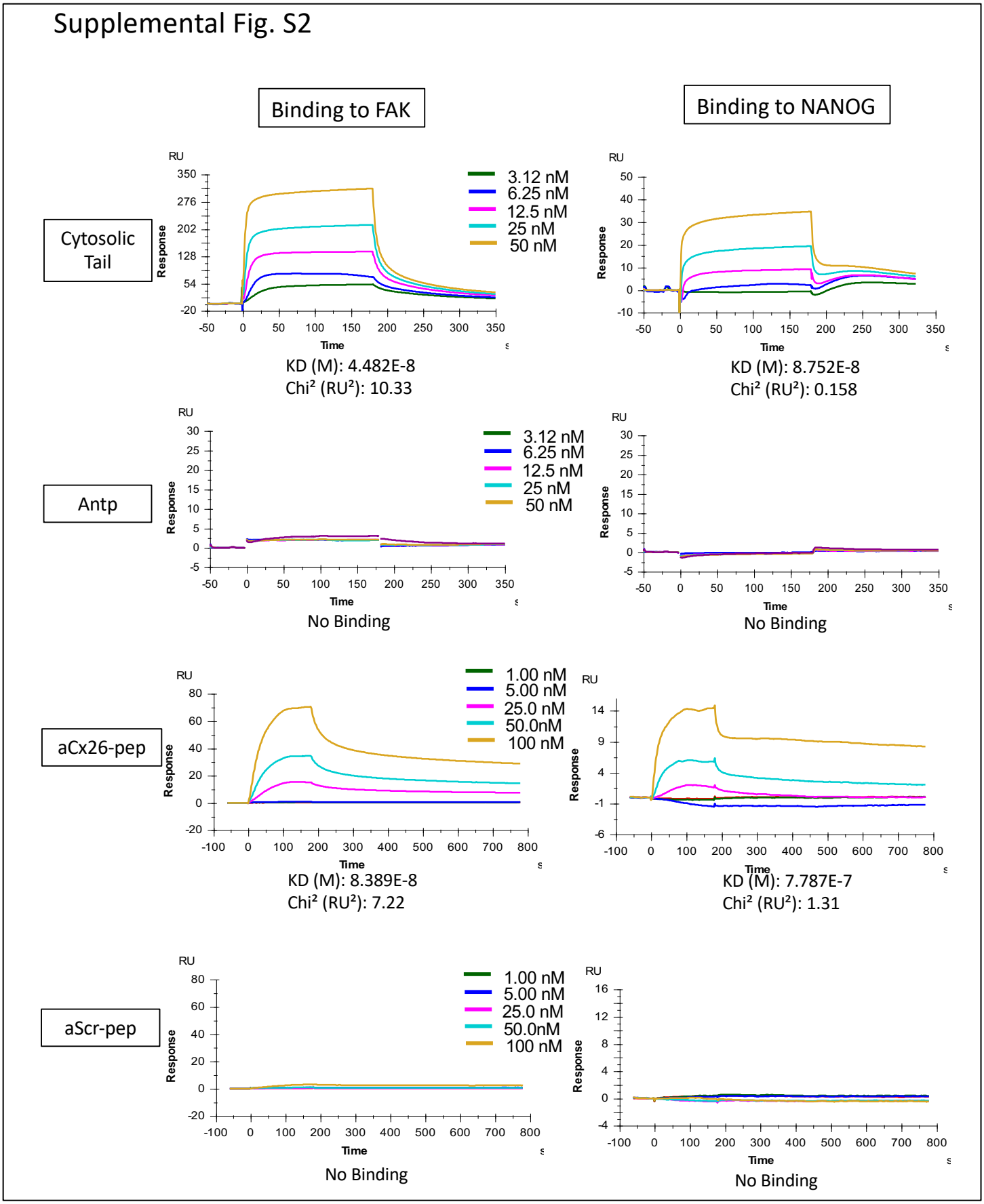

Supplemental Figure 2. SPR sensograms demonstrating binding of Cx26 peptides to FAK or NANOG proteins.

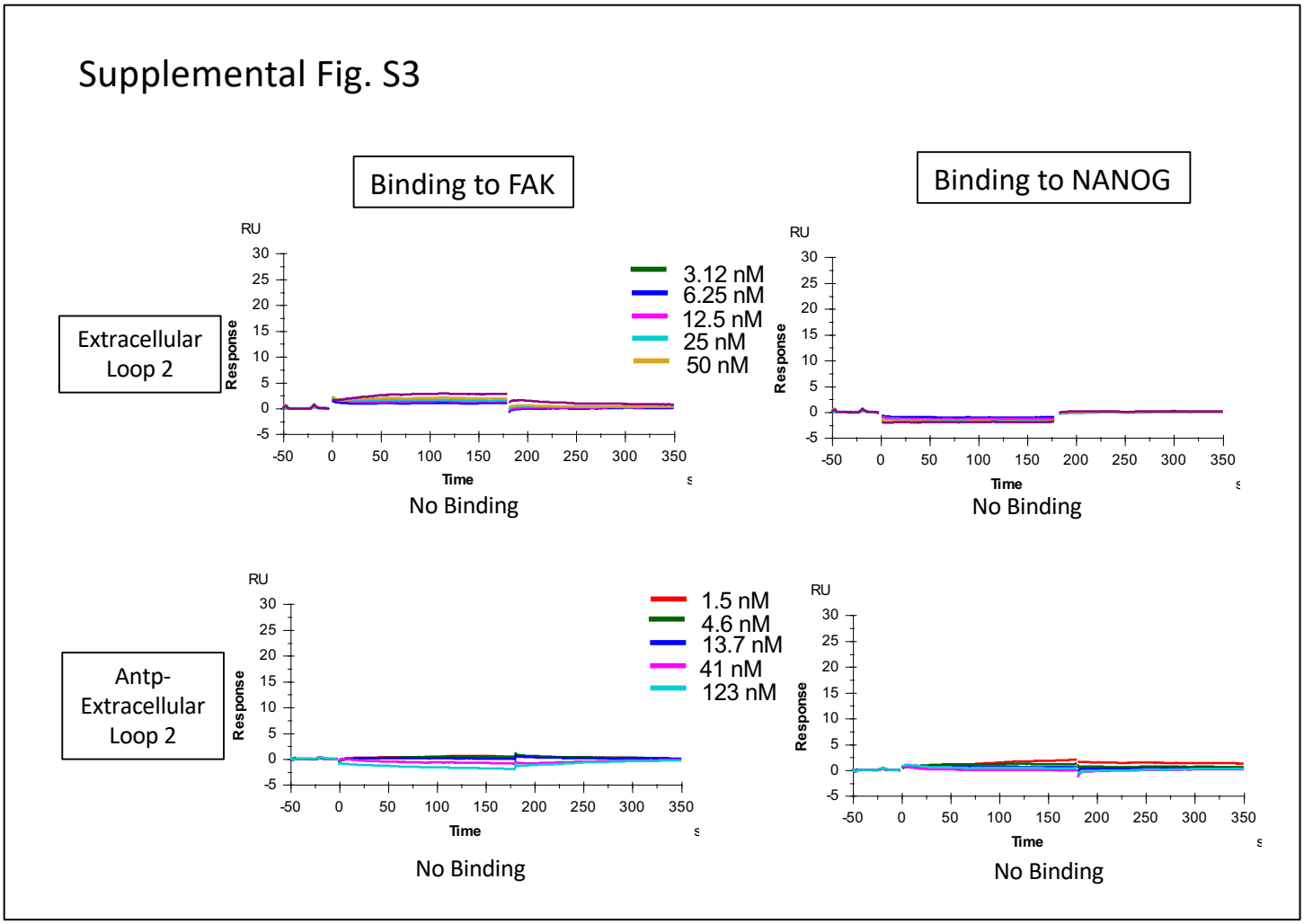

Supplemental Figure 3 SPR sensograms demonstrating no binding of Cx26 extracellular loop peptides to FAK or NANOG proteins.

Supplemental Tables.

Supplemental Table S1

Supplemental Table 1. FAK and NANOG binds to amino acids 216-220 of the Cx26 cytosolic tail.

Name	Sequence	NANOG	FAK
Wildtype	RYCSGKSKKPV	1.80^{-7} M	1.49^{-5} M
xR216	XYCSGKSKKPV	5.38^{-7} M	2.0^{-5} M
xRY	XXCSGKSKKPV	8.76^{-6} M	1.94^{-6} M
221-226	XXXXXKSKKPV	> 1.00 M	> 1.00 M
216-220	RYCSGXXXXXX	6.40^{-9} M	4.5^{-7} M
xV226	RYCSGKSKKPX	2.10^{-7} M	2.03^{-5} M

Supplemental Table S2

Supplemental Table 2. Summary of spheroid formation frequency following treatment with aCx26-pep and controls following a 14-day treatment of MDA-MB-231, MDA-MB-468, HCC70, and MCF7 cells.

Cell Line	Peptide Treatment	Confidence intervals for 1/(stem cell frequency)			p-value
		Lower	Estimate	Upper	
MDA-MB-231	Vehicle	4.39	2.3	1.4	-
MDA-MB-231	Antp	7.27	3.7	2.37	n.s.
MDA-MB-231	aScr-pep	8.43	4.73	2.78	n.s.
MDA-MB-231	aCx26-pep	427.39	104.7	25.94	4.0e-12
MDA-MB-468	Vehicle	14.6	8.2	4.8	-
MDA-MB-468	Antp	20.4	11.2	6.3	n.s.
MDA-MB-468	aScr-pep	17	9.46	4.7	n.s.
MDA-MB-468	aCx26-pep	1514.6	211.5	29.9	6.7e-5
HCC70	Vehicle	2.1	1.2	1.0	-
HCC70	Antp	4.4	2.3	1.4	n.s.
HCC70	aScr-pep	4.3	2.31	1.4	n.s.
HCC70	aCx26-pep	118.1	45.1	17.5	6.2e-13
MCF7	Vehicle	3.9	2.0	1.3	-
MCF7	Antp	2.1	1.2	1.0	n.s.
MCF7	aScr-pep	6.12	3.35	1.97	n.s.
MCF7	aCx26-pep	7.27	4.0	2.3	n.s.

Supplemental Table S3

Supplemental Table 3 . Primers used for qPCR.

Gene Name	Direction	Sequence (5'-3')
FABP5	Forward	TGA AGG AGC TAG GAG TGG GAA
	Reverse	TGC ACC ATC TGT AAA GTT GCA G
KRT18	Forward	GGC ATC CAG AAC GAG AAG GAG
	Reverse	ATT GTC CAC AGT ATT TGC GAA GA
KRT19	Forward	AAC GGC GAG CTA CAG GTG A
	Reverse	GGA TGG TCG TGT AGT AGT GGC
NRP2	Forward	GCT GGC TAT ATC ACC TCT CCC
	Reverse	TCT CGA TTT CAA AGT GAG GGT TG
PIN1	Forward	TGC CAC CGT CAC ACA GTA TT
	Reverse	CTG ACC AGG CCT TCT CTT TG
POSTN	Forward	CTC ATA GTC GTA TCA GGG GTC G
	Reverse	ACA CAG TCG TTT TCT GTC CAC
TAGLN	Forward	AGT GCA GTC CAA AAT CGA GAA G
	Reverse	CTT GCT CAG AAT CAC GCC AT